NRC Research Press

NOTE

Effect of dissolution on the load–settlement behavior of shallow foundations

Minsu Cha and J. Carlos Santamarina

Abstract: Mineral dissolution and solid–liquid phase change may cause settlement or affect the bearing capacity of shallow foundations. The effect of gradual grain dissolution on small-scale shallow foundation behavior is investigated using the discrete element method. Results show that dissolution is most detrimental during early stages, as initially contacting particles shrink and force chains must reform throughout the medium. Porosity tends to increase during dissolution and force chains evolve into strong localized forces with a honeycomb topology. Higher settlements are required to mobilize bearing resistance in post-dissolution sediments than in pre-dissolution ones. Subsurface mineral dissolution beneath a footing under load is the worst condition; in fact, settlements in such cases are higher than when a foundation load is applied on a sediment that has already experienced dissolution.

Key words: mineral dissolution, shallow foundation, discrete element method, footing load–displacement behavior.

Résumé : La dissolution de minéraux et le changement de phase solide-liquide peuvent causer un tassement ou influer la capacité portante des fondations superficielles. L'effet de la dissolution progressive de grains sur le comportement de fondation superficielle à petite échelle est étudié à l'aide de la méthode à éléments discrets. Des résultats montrent que la dissolution est plus nuisible au cours des premiers stades puisque les particules contactées initialement rétrécissent et des chaînes de force doivent se réformer tout au long du milieu. La porosité a tendance à augmenter au cours de la dissolution et les chaînes de force se transforment en une force localisée avec une topologie en nid d'abeille. Des tassements supérieurs sont nécessaires pour mobiliser la résistance de roulement dans les sédiments à post-dissolution contrairement aux sédiments à pré-dissolution. La dissolution de minéraux en sous-surface sous un empattement sous charge est le plus mauvais état; en fait, les tassements dans ce cas sont supérieurs quand une charge de fondation est appliquée sur un sédiment qui a déjà connu une dissolution. [Traduit par la Rédaction]

Mots-clés : dissolution de minéraux, fondation superficielle, méthode d'éléments discrets, comportement de déplacement d'empattement sous charge.

Introduction

A firm foundation can be compromised by dissolution-driven solid mass loss and volume contraction. Examples extend beyond the common case of carbonates and karst terrain, and include foundations built in cold regions that are subject to ground thawing, offshore structures founded on hydrate-bearing marine sediments, and mineral dissolution in CO_2 geological storage projects. Even low-reactivity minerals could compromise the performance of critical infrastructure with long design lives such as dams and waste repositories. Furthermore, there are other mechanisms for internal volume contraction that may have macroscale implications similar to mineral dissolution, such as loess collapse upon wetting (Haq and Kibria 1994; Houston et al. 2001; Rinaldi et al. 1998; Rodrigues and de Lollo 2007).

Particle-scale dissolution affects small- and large-strain properties. The sediment contracts yet the void ratio increases during dissolution (Cha and Santamarina 2014; Fam et al. 2002; McDougall et al. 2013; Muir Wood et al. 2010; Shin and Santamarina 2009; Tran et al. 2012; Truong et al. 2010), and a "honeycomb fabric" emerges (Shin and Santamarina 2009; Shin et al. 2008). The value of the coefficient of earth pressure at rest, k_o, decreases often to the coefficient of active earth pressure, k_a, before it recovers (experiments in Shin and Santamarina 2009; simulations in Cha and Santamarina 2014), and shear wave velocity decreases and attenuation increases during dissolution (Fam et al. 2002; Truong et al. 2010). The peak friction angle is lower after dissolution (Fam et al. 2002; Tran et al. 2012), and the cone penetration resistance decreases with increasing dissolution (Cha and Santamarina 2013).

The effects of gradual grain dissolution on the load-settlement response of shallow foundations are explored herein using the discrete element method. We consider two distinct histories: footing "load before dissolution" and "dissolution before load". The numerical simulation study assumes homogeneously distributed soluble grains throughout the medium (this is one of various dissolution patterns observed in nature). In addition, simulations effectively represent a small-scale 1g model rather than a full-scale footing; however, results provide unique insight on load–dissolution phenomena relevant to field situations.

Numerical simulation

Figure 1 shows the test geometry and boundary conditions; simulation parameters are summarized in Table 1. Details follow.

Geometry and boundaries

The design of the discrete element simulation takes into consideration previous model results to minimize scale effects: (*i*) the

Received 28 August 2014. Accepted 2 March 2016.

M. Cha. Department of Civil Engineering, Texas A&M University, 3136 TAMU, College Station, TX 77843-3136, USA.
J.C. Santamarina. Earth Science and Engineering, King Abdullah University of Science and Technology (KAUST), Thuwal 23955-6900, Saudi Arabia.
Corresponding author: Minsu Cha (email: mcha@tamu.edu).

Fig. 1. Discrete element modelling study: problem geometry and boundary conditions. (Note: soluble particles are shown in red; SF = 10%: 1057 out of 10 567 disks.) [Color online.]

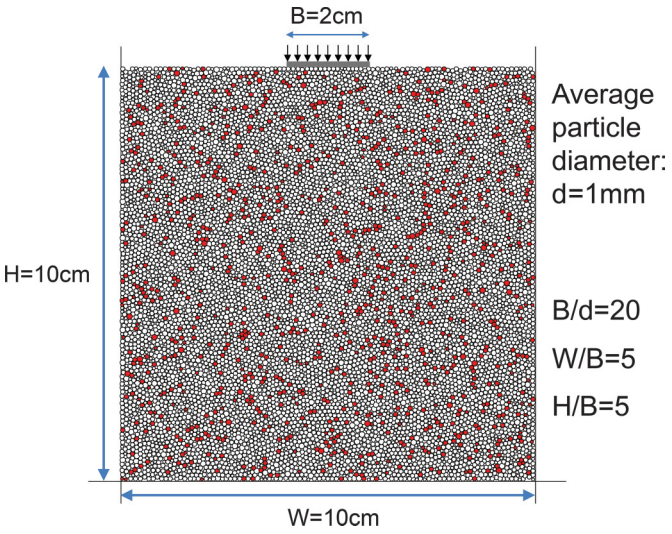

Table 1. Simulation parameters: two-dimensional discrete element code (PFC-2 D).

	Property	Value
Grains (disks)	Initial radius of disks	Uniform size distribution (R_{min} = 0.4 mm, R_{max} = 0.6 mm)
	Number of disks	10 567
	Mass density of disks (kg/m^3)	2650
	Linear contact model	
	Normal stiffness, k_n (N/m)	10^8
	Shear stiffness, k_s (N/m)	10^8
	Interparticle friction	0.5
	Hindered rotation, HR (%)	0, 40, 80
	Number of dissolvable particles	1057 (10%)
Boundary conditions	Initial specimen dimension (height × width)	10 cm × 10 cm
	Upper surface boundary	Free
	Lateral strain	0
	Particle-to-wall friction	0

ratio of the footing width, B, to the soil mean grain size, d, is $B/d = 20$ (Kusakabe 1995; Lau and Bolton 2011); (*ii*) the ratio of the depth from the footing to bedrock, H, to the footing width, B, is $H/B = 5$ (Cerato and Lutenegger 2006); and (*iii*) the ratio of the footing width, B, to the distance to lateral boundaries, W, is $B/W = 5$ (Davis and Selvadurai 2002). Even with these tight boundaries, this two-dimensional model involves 10 567 grains, to which the study is limited due to computational expenses in dissolution and loading on unstable, sensitive post-dissolution specimens (note: we do not use symmetry along the centerline to avoid preferential grain alignment against straight boundaries; similarly, we do not use periodic lateral boundary conditions because it biases the stress field). There is no friction between the sediment and walls, or between the sediment and footing plate.

Approach and procedure

Randomly positioned frictionless disks are allowed to grow to their target size (uniform size distribution: minimum radius R_{min} = 0.4 mm to maximum radius R_{max} = 0.6 mm). Then, interparticle friction and gravity are turned-on under zero lateral strain boundary conditions $\varepsilon_h = 0$. Angularity and interlocking are captured by hindering the rotation of a selected fraction of particles. Spherical particles rotate more freely than nonspherical ones found in real sediments where interlocking inhibits rotation. Although particle rotation has a limited effect on elastic properties, it alters shear resistance and volume change (Bardet 1994; Iwashita and Oda 1998; Mohamed and Gutierrez 2010). In this study, rotation is hindered on pre-selected particles as a numerical proxy for angularity and interlocking (Bardet 1994; Iwashita and Oda 1998; Suiker and Fleck 2004). Three different fractions of particles with hindered rotation, HR (%), are considered: HR = 0% (without hindered rotation), 40%, and 80% (see Cha and Santamarina (2014) for a discussion of this numerical proxy). The linear contact model is used for this two-dimensional study (O'Sullivan 2011).

Soluble particles are randomly selected: the mass fraction, SF, of soluble particles is 10% in all these simulations. Dissolution under zero lateral strain is simulated by gradually reducing the radius of all the soluble particles at the same rate. The gradual size reduction is performed by numerous steps of minute size reduction (radius reduction of 1/50 000 times initial radius in each step), each step followed by a full equilibrium stage. In particular, the ratio of the mean unbalanced force to the mean contact force is always smaller than 0.001 to ensure stable conditions throughout the dissolution processes.

Load–dissolution histories

Load–settlement simulations are done in stress-controlled mode by increasing the load in small steps. Simulations are performed for three load–dissolution histories: (*i*) load–settlement tests on original pre-dissolution sediments loaded to failure; (*ii*) load–settlement tests on post-dissolution sediments, in which case the dissolution takes place before load application; and (*iii*) loading to a factor of safety FS ~ 2.5 followed by grain dissolution under constant vertical load.

Results

Preliminary study

The macroscale friction angle, ϕ, for different degrees of hindered rotation, HR, is determined in a preliminary set of tests designed to measure the angle of repose. Results show that ϕ = 22°, 35°, and 48° for HR = 0%, 40%, and 80%, respectively. These results highlight the effect of rotational frustration — typically associated with angularity and interlocking — on the soil friction angle (see additional results in Cha 2012). Numerical results obtained for the three load–dissolution histories are reported next.

Case 1: Load before dissolution

The load–deformation response obtained for footings on soils with different angularity HR are plotted in Fig. 2. The three cases show high initial stiffness. Similar to field tests, resistance continues to increase as the footing settles. Consider the footing bearing capacity, q_{ult}, as the load at a normalized settlement $\delta/B \sim 20\%$, where δ is the settlement (Lee and Salgado 2005; Loukidis and Salgado 2011; Mayne and Illingworth 2010). The measured q_{ult} values reflect the pronounced effect friction angle has on bearing capacity; in fact, when compared with free rotation (HR = 0%, ϕ = 22°), bearing capacity at $\delta/B \sim 20\%$ is ~3 times higher when hindered rotation is HR = 40% (ϕ = 35°) and 16 times higher when HR = 80% (ϕ = 48°). These results are approximately in line with the exponential increase in bearing capacity with increasing friction angle predicted by analytical solutions.

Case 2: Load after dissolution

The load–settlement response for the footing on post-dissolution sediments shows lower stiffness (in agreement with lower stiffness observed in simple shear simulations reported in Cha and Santamarina (2014) and gradual settlement from the onset of loading (Fig. 2). Load after dissolution requires significantly larger settlements to mobilize internal friction to achieve the same capacity than load before dissolution.

Fig. 2. Footing load versus Settlement, load-controlled simulation: (*a*) HR = 0%; (*b*) HR = 40%; (*c*) HR = 80%. (Note: black circle on *x*-axis indicates surface settlement in the absence of a footing observed at end of dissolution. Green square on *x*-axis adds to the black circle the settlement that footing experiences at $q = q_{all}$ when loaded after dissolution.) [Color online.]

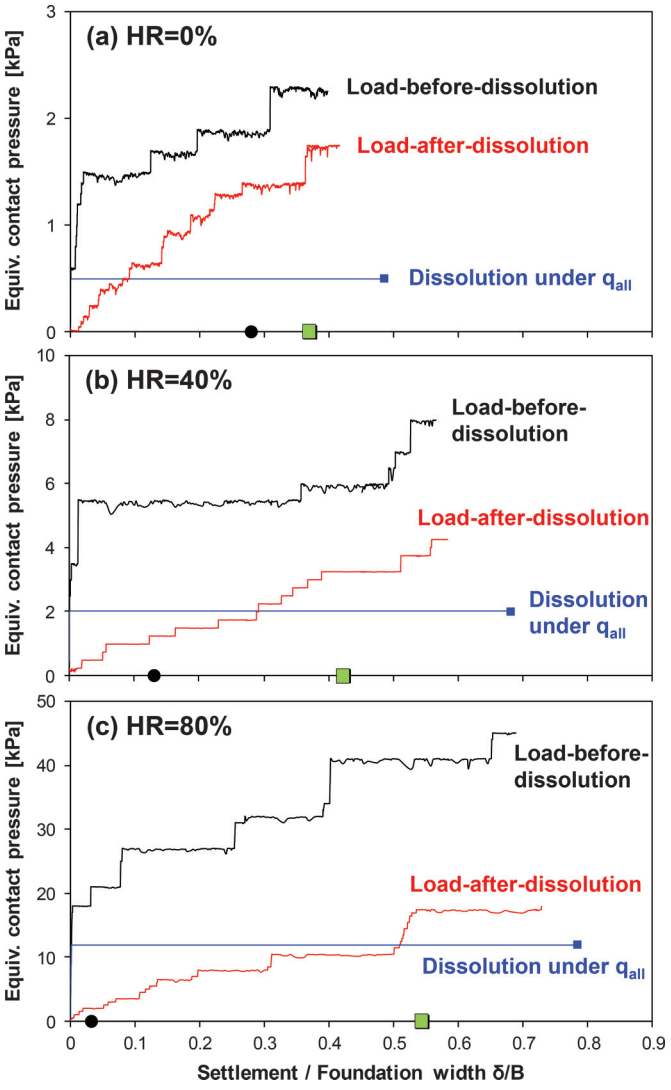

Case 3: Dissolution under a constant footing load

Finally, consider the case when the footing sitting on the original pre-dissolution soil is loaded to an allowable load, q_{all}, that corresponds to a factor of safety FS = $q_{all}/q_{ult} \approx 2.5$; then, the sediment is subjected to dissolution while keeping the footing load q_{all} constant. Figure 3 shows the dissolution-induced settlement at constant load q_{all} as a function of the size reduction $\Delta R/R_0$ soluble particles experience (where ΔR and R_0 are the change in radius and initial radius, respectively), i.e., a proxy of dissolution time. During early stages of dissolution, settlement is almost linear with size reduction and dissolution is most detrimental to the sediment structure as initially contacting particles shrink and force chains must reform throughout the medium. The more frictional sediment (e.g., HR = 80%) shows sudden displacement due to collapse of pronounced arching in more frictional sediment under dissolution. Most of the settlement occurs before $\Delta R/R_0 < 60\%$. During later stages, small dissolving particles fall within voids and additional dissolution does not affect the load-carrying granular skeleton.

Comparison

Results superimposed on Fig. 2 for all levels of interlocking and load–dissolution histories show similar relative trends. The black circle on the *x*-axis shows the settlement in the soil mass during dissolution without the footing; the green square on the *x*-axis adds to the black dot the settlement the footing experiences in load after dissolution when the footing load is $q = q_{all}$. It can be seen that dissolution under an existing foundation load (blue line) causes a final settlement that is greater than the total settlement the sediment accumulates during dissolution followed by loading (green square).

Figure 4 shows grain displacement vectors for all three load–dissolution histories in the same scale for the case of free rotation HR = 0%. Displacements during pre- and post-dissolution loading are concentrated near the footing (Figs. 4*a* and 4*b*). Particle movements are the highest during dissolution under a constant load, affecting particles at greater depth, and causing significant upward grain flow away from the footing (Fig. 4*c*). Note that, in Fig. 4*c*, particle movements due to dissolution are subtracted from total movements, so that only particle movements due to the foundation loading appear and thus the magnitude of particle displacements can be compared with Figs. 4*a* and 4*b*. See Figs. S3 and S4 in the supplementary data[1] = 40% and 80%.

The internal fabric in the original pre-dissolution sediments is characterized by low porosity ($n = 0.168$) and distributed contact force chains (Fig. 4*a*). On the other hand, the post-dissolution sediments have higher porosity ($n = 0.204$ for HR = 0%, $n = 0.230$ for HR = 40%, and $n = 0.245$ for HR = 80%), and exhibit "honeycomb-shaped" larger force chain circles that lead to lower stiffness and higher compressibility (Shin and Santamarina 2009; Tordesillas 2007; Tordesillas et al. 2011) (Figs. 4*b* and 4*c*).

Boundary effects

While $H/B = 5$ is within the recommendations by previous literature, $B/W = 5$ may be marginal and create boundary effects. The force exerted by particles at the side walls increases with foundation pressure (Fig. S1; refer to supplementary data for Figs. S1–S4 mentioned in this paragraph),[1] which indicates boundary effects. Higher wall forces are created with more frictional specimens as higher foundation pressure is applied to reach capacity (Fig. S1*b*), which may increase the boundary effect. Lateral extent of the shear failure surface is greater as the friction angle increases, thus the interaction of the passive zones and spiral slip surface with walls should be more prominent in specimens with a higher internal friction angle. Figure S2 shows the specimen with a higher friction angle, creating a larger failure surface and interacting more with boundaries. Marked granular interaction with lateral boundaries is also observed when large deformation is created during dissolution under load (q_{all}) (Figs. 4*c*, S3*c*, and S4*c*). In laboratory tests, rigid lateral walls normally overestimate capacity by their confining effect. However, no friction at the walls in our simulations may offset the boundary confinement to some degree, e.g., contact force chains are relatively weak at passive zones and near the end of the spiral surface toward the walls in Figs. 4*c*, S3*c*, and S4*c*. In the same context, in Fig. S2*b*, particles are free to move upward at the end of the spiral surface due to frictionless walls. Proper quantification of the boundary effect on the load–settlement behavior requires systematic calibration using numerical chambers.

[1]Supplementary data are available with the article through the journal Web site at http://nrcresearchpress.com/doi/suppl/10.1139/cgj-2014-0370.

Fig. 3. Settlement versus normalized grain size reduction for dissolution under constant load q_{all} for all three levels of imposed hindered rotation. (Note: the three simulations are run at different loads q_{all}, but at the same factor of safety.)

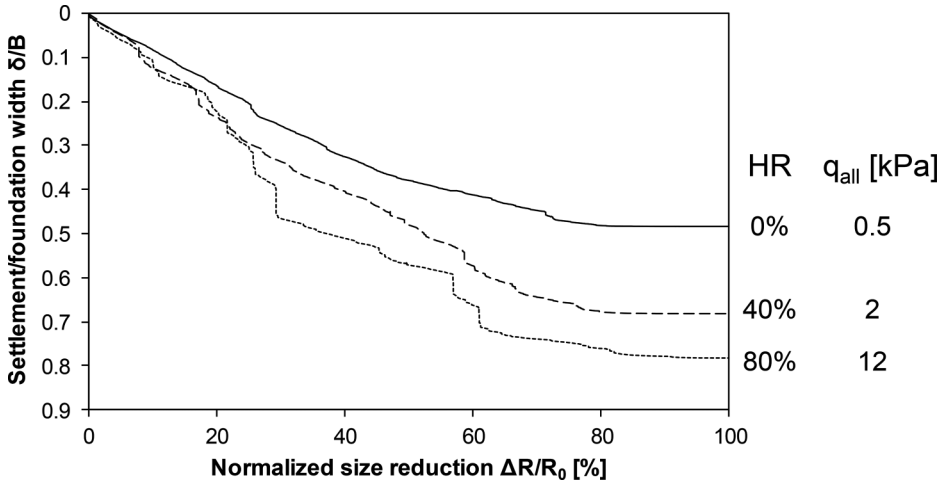

Fig. 4. Contact force chains and displacement vectors for the three cases at the same foundation load q = 0.5 kPa (case: hindered rotation HR = 0%): (*a*) load before dissolution; (*b*) load after dissolution; (*c*) dissolution at constant load q_{all}. (Displacement vectors and contact force chains are shown at the same scales.) [Color online.]

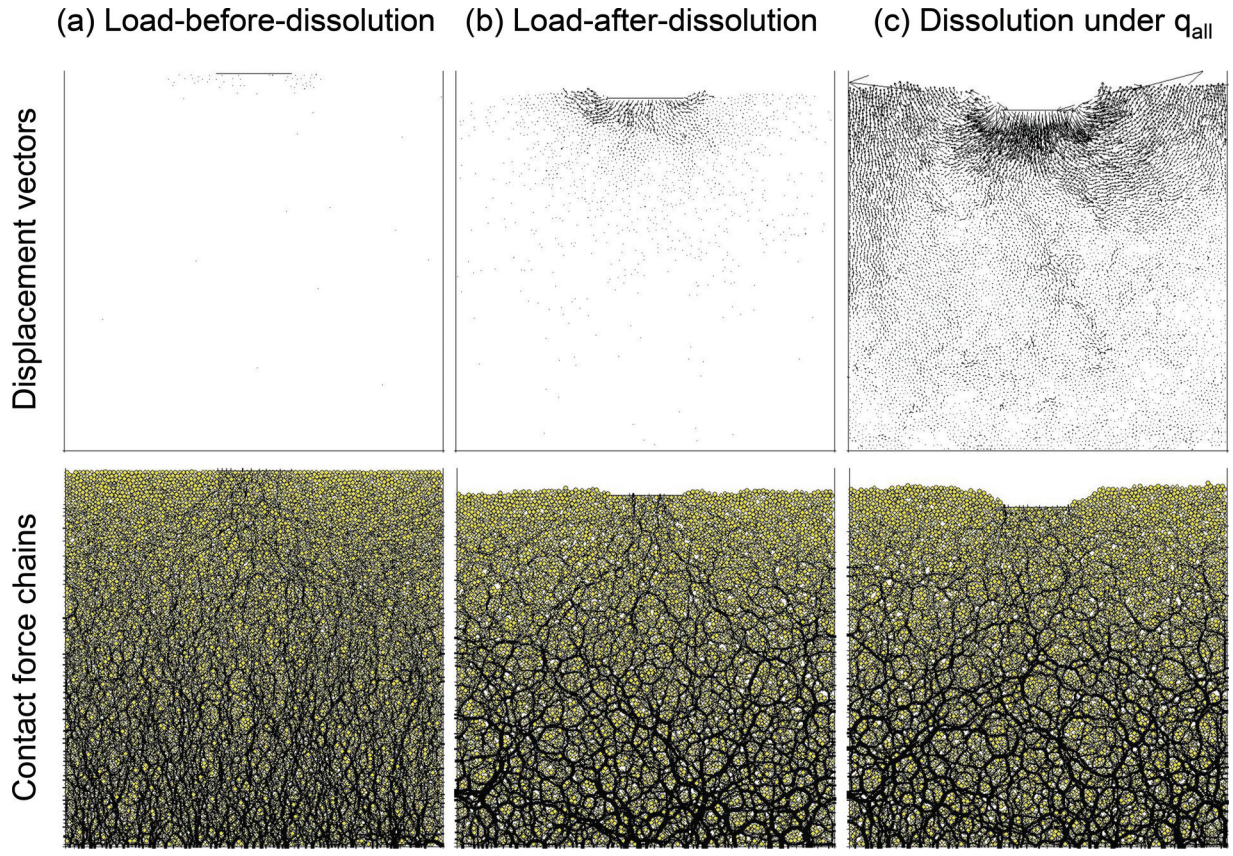

Conclusions

Mineral dissolution affects sediment internal structure and the load–settlement response footings experience. When dissolving grains are homogenously distributed throughout the medium, dissolution is most detrimental during early stages as initially contacting particles shrink and force chains must reform throughout the medium.

Porosity tends to increase during dissolution; in fact, the higher the sediment internal friction, the higher the final porosity after dissolution in the stress regime explored in this paper. Furthermore, force chains evolve into strong localized forces with a honeycomb topology.

Higher settlements are required to mobilize the same bearing resistance in post-dissolution sediments than in pre-dissolution ones. Grain angularity and interlocking significantly increases the overall load capacity on sediments either before or after dissolution. Subsurface mineral dissolution beneath a footing under load is the worst condition; in fact, settlements in this case are higher

than when a foundation load is applied on a sediment that has already experienced dissolution.

Acknowledgements

Support for this research was provided by the Department of Energy Savannah River Operations Office led by B. Gutierrez. Additional support was provided by the Goizueta Foundation. F.J. Santamarina edited the manuscript. The authors are grateful to the anonymous reviewers for their valuable comments.

References

Bardet, J.P. 1994. Observations on the effects of particle rotations on the failure of idealized granular materials. Mechanics of Materials, **18**(2): 159–182. doi:10.1016/0167-6636(94)00006-9.

Cerato, A.B., and Lutenegger, A.J. 2006. Bearing capacity of square and circular footings on a finite layer of granular soil underlain by a rigid base. Journal of Geotechnical and Geoenvironmental Engineering, **132**(11): 1496–1501. doi:10.1061/(ASCE)1090-0241(2006)132:11(1496).

Cha, M. 2012. Mineral dissolution in sediments. Ph.D. thesis, School of Civil and Environmental Engineering, Georgia Institute of Technology, Atlanta, Ga.

Cha, M., and Santamarina, J.C. 2013. Predissolution and postdissolution penetration resistance. Journal of Geotechnical and Geoenvironmental Engineering, **139**(12): 2193–2200. doi:10.1061/(ASCE)GT.1943-5606.0000949.

Cha, M., and Santamarina, J.C. 2014. Dissolution of randomly distributed soluble grains: post-dissolution k_0-loading and shear. Géotechnique, **64**(10): 828–836. doi:10.1680/geot.14.P.115.

Davis, R.O., and Selvadurai, A.P.S. 2002. Plasticity and geomechanics. Cambridge University Press, Cambridge, UK, New York.

Fam, M.A., Cascante, G., and Dusseault, M.B. 2002. Large and small strain properties of sands subjected to local void increase. Journal of Geotechnical and Geoenvironmental Engineering, **128**(12): 1018–1025. doi:10.1061/(ASCE)1090-0241(2002)128:12(1018).

Haq, I.U., and Kibria, S. 1994. Engineering characteristics of arid soils. *In* Proceedings of the 1st International Symposium on Engineering Characteristics of Arid Soils. *Edited by* P.G. Fookes and R.H.G. Parry. A.A. Balkema, London. pp. 91–93.

Houston, S.L., Houston, W.N., Zapata, C.E., and Lawrence, C. 2001. Geotechnical engineering practice for collapsible soils. Geotechnical and Geological Engineering, **19**(3): 333–355. doi:10.1023/A:1013178226615.

Iwashita, K., and Oda, M. 1998. Rolling resistance at contacts in simulation of shear band development by DEM. Journal of Engineering Mechanics, **124**(3): 285–292. doi:10.1061/(ASCE)0733-9399(1998)124:3(285).

Kusakabe, O. 1995. Chapter 6: Foundations. *In* Geotechnical centrifuge technology. *Edited by* R.N. Taylor. Blackie Academic & Professional, London. pp. 118–167.

Lau, C.K., and Bolton, M.D. 2011. The bearing capacity of footings on granular soils. II: Experimental evidence. Géotechnique, **61**(8): 639–650. doi:10.1680/geot.7.00207.

Lee, J., and Salgado, R. 2005. Estimation of bearing capacity of circular footings on sands based on cone penetration test. Journal of Geotechnical and Geoenvironmental Engineering, **131**(4): 442–452. doi:10.1061/(ASCE)1090-0241(2005)131:4(442).

Loukidis, D., and Salgado, R. 2011. Effect of relative density and stress level on the bearing capacity of footings on sand. Géotechnique, **61**(2): 107–119. doi:10.1680/geot.8.P.150.3771.

Mayne, P.W., and Illingworth, F. 2010. Direct CPT method for footing response in sands using a database approach. *In* Proceedings of the 2nd International Symposium on Cone Penetration Testing., Huntington Beach, Calif.

McDougall, J., Kelly, D., and Barreto, D. 2013. Particle loss and volume change on dissolution: experimental results and analysis of particle size and amount effects. Acta Geotechnica, **8**(6): 619–627. doi:10.1007/s11440-013-0212-0.

Mohamed, A., and Gutierrez, M. 2010. Comprehensive study of the effects of rolling resistance on the stress-strain and strain localization behavior of granular materials. Granular Matter, **12**(5): 527–541. doi:10.1007/s10035-010-0211-x.

Muir Wood, D., Maeda, K., and Nukudani, E. 2010. Modelling mechanical consequences of erosion. Geotechnique, **60**(6): 447–457. doi:10.1680/geot.2010.60.6.447.

O'Sullivan, C. 2011. Particulate discrete element modelling: a geomechanics perspective. Taylor & Francis, New York.

Rinaldi, V.A., Redolfi, E.R., and Santamarina, J.C. 1998. Characterization of collapsible soils with combined geophysical and penetration testing. *In* Proceedings of the 1st International Conference on Site Characterization (ISC 98). *Edited by* P.K. Robertson and P.W. Mayne. A.A. Balkema Publishers, Atlanta, Ga. pp. 581–588.

Rodrigues, R., and de Lollo, J. 2007. Influence of domestic sewage leakage on the collapse of tropical soils. Bulletin of Engineering Geology and the Environment, **66**(2): 215–223. doi:10.1007/s10064-006-0065-y.

Shin, H., and Santamarina, J.C. 2009. Mineral dissolution and the evolution of k_0. Journal of Geotechnical and Geoenvironmental Engineering, **135**(8): 1141–1147. doi:10.1061/(ASCE)GT.1943-5606.0000053.

Shin, H., Santamarina, J.C., and Cartwright, J.A. 2008. Contraction-driven shear failure in compacting uncemented sediments. Geology, **36**(12): 931–934. doi:10.1130/G24951A.1.

Suiker, A.S.J., and Fleck, N.A. 2004. Frictional collapse of granular assemblies. Journal of Applied Mechanics, **71**(3): 350–358. doi:10.1115/1.1753266.

Tordesillas, A. 2007. Force chain buckling, unjamming transitions and shear banding in dense granular assemblies. Philosophical Magazine, **87**(32): 4987–5016. doi:10.1080/14786430701594848.

Tordesillas, A., Lin, Q., Zhang, J., Behringer, R.P., and Shi, J.Y. 2011. Structural stability and jamming of self-organized cluster conformations in dense granular materials. Journal of the Mechanics and Physics of Solids, **59**(2): 265–296. doi:10.1016/j.jmps.2010.10.007.

Tran, M.K., Shin, H., Byun, Y.-H., and Lee, J.-S. 2012. Mineral dissolution effects on mechanical strength. Engineering Geology, **125**: 26–34. doi:10.1016/j.enggeo.2011.10.014.

Truong, Q.H., Eom, Y.H., and Lee, J.S. 2010. Stiffness characteristics of soluble mixtures. Géotechnique, **60**(4): 293–297. doi:10.1680/geot.8.T.032.